Computational Design Optimization of a Smart Material Shape Changing Building Skin Tile

Robert J. Zupan[1], Jing Xu[2], Richard V. Beblo[3], Dale T. Clifford[4], Ankush Aggarwal[5], and John C. Brigham[6]

[1]PhD Student, Dept. of Civil and Environmental Engineering, Univ. of Pittsburgh, Email: rjz6@pitt.edu (corresponding author)

[2]PhD Student, Dept. of Civil and Environmental Engineering, Univ. of Pittsburgh, Email: jix57@pitt.edu

[3]PhD, Research Engineer, University of Dayton Research Institute, Email: richard.beblo.1@us.af.mil

[4]PhD, Associate Professor, College of Architecture and Environmental Design, California Polytechnic State Univ., Email: dtcliffo@calpoly.edu

[5]PhD, Lecturer, School of Engineering, Univ. of Glasgow, Email: Ankush.Aggarwal@glasgow.ac.uk

[6]PhD, Professor, Dept. of Engineering, Durham Univ., Email: john.brigham@durham.ac.uk

ABSTRACT

The development and evaluation of a computational approach for optimal design of a smart material shape changing building skin is presented and numerically evaluated. Specifically, a unique shape-based approach is utilized to create an optimization approach to identify the activation and actuation mechanisms to minimize the difference between a desired shape and the estimated morphed shape. Three potential metrics of shape difference are considered and their capability to facilitate an efficient optimization process leading to accurate shape matching is evaluated. Details of the optimal design framework are presented, particularly focusing on the shape difference

metrics as well as the strategy to parameterize the activation of the smart material. In particular, the parameterization strategy is a unique approach to easily integrate controllable localized activation within a smart material structure in a generally applicable way that does not limit the design search space. A series of numerical design examples are presented based on the concept of a smart material (e.g., shape memory polymer) shape changing tile that can be activated and actuated in a variety of ways to achieve desirable surface wrinkle patterns. These numerical design examples are applied to both 2D and 3D problems and consider a variety of parameterizations and target shapes. Results indicate that the shape-based approach can consistently determine the mechanisms of morphing needed to accurately match a target shape. Furthermore, it is shown that localized material activation can lead to not only a more accurate shape but also requires less energy and actuation devices to do so.

Keywords: Self-shading, Smart Material, Optimization, Objective Function, Hausdorff, Computational Mechanics

INTRODUCTION

Responsive building skins have been shown to have effects on all the main energy consumers of commercial buildings: lighting, ventilation, and heating and cooling (Shameri et al. 2011). Examples include the skin used on the Media-TIC building (Dewidar et al. 2013), which uses a light sensor to measure thermal loads on a building and inflates portions of the skin in order to increase insulation during times of high thermal loading, and the Heliotrace system (Dewidar et al. 2013) and the responsive skin of the Al Bahar towers (Cilento 2012), which both utilize a series of mechanical apertures that open or close portions of the skin, allowing different amounts of light to enter the building. In most cases the current technologies are binary, either activated or inactivated based on a stimulus threshold, or have a limited number of configurations. Thus, significant work still remains to achieve technologies that can adapt to multiple environmental states and have a higher level of customization. One possibility proposed to increase functionality of responsive building façade is the integration of smart materials (Jani et al. 2014; Mather et al. 2009; Lampert 2004; Otsuka and Wayman 1999).

The technologies being developed for shape changing building skins that use smart materials have primarily relied upon passive mechanisms, in that the shape change that occurs is caused by the material being activated by changes in the surrounding environmental conditions (e.g., moisture change (Holstov et al. 2015) or temperature change (Barrett and Barrett 2016)). Passive use of the smart material has the benefit of not requiring any additional intervention or energy costs to the user beyond maintenance requirements. Yet, passive use of the material may limit the extent that the behavior of the structure can be customized and may limit feasibility of certain applications or material types if the activating environmental condition does not correlate with the desired material change. Alternatively, active use of smart materials for shape changing structures that include a mechanism to apply activation energy and/or actuation to the structure have the obvious disadvantage of energy consumption, but can substantially increase the range of potential shape changes and the potential applications of the technology overall. There have been several application areas of smart material structures where this benefit of active use has outweighed the additional energy costs, such as morphing aircraft applications (Liu et al. 2014; Yu et al. 2009; Sun et al. 2015). Although active use of smart materials for shape changing structures can significantly expand the potential functions of the structure, this expansion can also substantially increase the initial challenge of designing the smart material structure.

With any degree of complexity in the desired behavior, the active use of smart materials for shape changing structures can include nearly infinite non-trivial potential design solutions, when potentially seeking to define localized stimulation/activation, a multitude of mechanical actuation methods, or even the use of multiple smart materials together. Such design problems are often best handled through a computational optimal design approach, which have already been used for several smart material structure design applications (Molinari et al. 2015; Woods and Friswell 2016; Liu et al. 2014; Yu et al. 2009; Sun et al. 2015; Lu and Kota 2003; Prock et al. 2002; Namgoong et al. 2006; Mohaghegh Motlagh 2014; Wang and Brigham 2012). Computational approaches are particularly beneficial for problems that have non-trivial and/or non-intuitive solutions, and complex objectives and constraints. Although substantial work has been done developing computational

design methods for various applications, with any new application there are new and unique challenges, ranging from the definition of the forward model and its parameterization to the quantification of the design objective and constraints.

The current study presents a computational framework for the design of the active mechanisms for a smart material building skin tile to optimally achieve a desired shape change. The target of shape change is chosen as it aligns with the prior work using hygromorphic structures (Bridgens 2018), which was noted to be largely for aesthetic reasons thus far, while also allowing for inclusion of other more functional objectives, such as increasing shading similar to the work in (Barrett and Barrett 2016). In other words, it is assumed that some prior analysis to define the desired combination of appearance and function has been performed to provide the target shape change to be designed toward. As such, one particular focus of the study is on determining an appropriate objective function for the design approach that quantifies the difference between the desired shape change and the shape change predicted by the forward model for the optimization procedure. In addition, focus is also placed on the strategy to define the unknown design parameters, particularly to ensure the localized activation is feasible to implement without sacrificing the shape change capability. Although more generally applicable, the design strategy is presented in the context of an example design of the mechanical actuation and material activation of tile entirely comprised of a homogeneous smart material. In the following section, the details of this exemplar smart material shape changing building skin tile are provided. In Section 3 the general computational inverse problem for the design of a smart material building skin tile is presented. Numerical examples, their results, and discussion are then given in Section 4, which is followed by concluding remarks in Section 5.

DESIGN CONCEPT

The design concept considered herein is an adaptive shape changing “wrinkled" surface tile based upon the prior work developing building surface “cactus tiles" by Clifford (Clifford 2019). The original cactus tile objective was to have static “wrinkled" surface tiles that were both aesthetically pleasing and had functional benefits in terms of self-shading. However, it is envisioned that adding

the capability of such tiles to change between wrinkle patterns, would further enhance the original benefits and potentially include many other functional behaviors (Clifford 2019; Zupan et al. 2017; Zupan et al. 2018). As shown in Figure 1, the proposed mechanism to produce a tile that can morph between different wrinkle patterns (i.e., shape changing cactus tile) is envisioned to be controllable activation of the smart material comprising the tile (e.g., softening) and mechanical actuation to deform the tile into a desired shape. For the sake of simplicity, this work does not consider the activation process (e.g., heat transfer process if thermal activation was used) and assumes that the deformed shape could be perfectly "locked in" once activation is removed. However, these behaviors could be included in the forward modeling in subsequent work without significant change to the computational design strategy. Similarly, the overall dimensions of the tile were assumed to be given/fixed. Thus, the remaining unknown variables to determine for the design of this tile concept are the locations and magnitude of mechanical actuation (i.e., applied force and/or displacement) and the location and size of the regions of the material to be activated.

DESIGN SOLUTION STRATEGY

The design strategy considered herein is based on utilizing non-linear optimization in combination with a numerical representation of the shape changing tile to be designed. As noted, the primary objective of the optimal design is to achieve a given desired shape change. In this work, the target shape was assumed to be defined as the desired outer surface shape of the tile. However, as is often the case with smart material applications, minimizing the energy cost of the shape changing process was also considered as an objective of the design. Thus, the design problem can be written in the general form of the following constrained optimization problem:

$$\begin{aligned} \underset{\vec{\gamma}}{\text{minimize:}} \quad & \{C\left(S_T, S_F(\vec{u})\right), E(\vec{u}, \vec{\gamma})\} \\ \text{subject to:} \quad & F(\vec{u}, \vec{\gamma}) = 0 \\ & \vec{b}_l \leq A(\vec{\gamma}) \leq \vec{b}_u, \end{aligned} \tag{1}$$

where S_T is the target surface shape, S_F is the predicted morphed shape of tile as defined by

the deformation of the tile, $\vec{u}$, estimated by the solution of the forward problem, $F(\vec{u}, \vec{\gamma}) = 0$ (i.e., the partial differential equation constraint), for a given set of actuation and activation design parameters, $\vec{\gamma}$, $C(\cdot, \cdot)$ is the metric that quantifies the difference between two shapes, $E(\vec{u}, \vec{\gamma})$ is the estimated energy consumption required to complete the shape change process, $\vec{b}_l$ and $\vec{b}_u$ are the lower and upper bound constraint vectors, respectively, and $A(\vec{\gamma})$ is the operator that forms the necessary constraint equations involving the design parameters. Note that this is the general form of the optimization problem considered herein, and the examples will more specifically state the respective components, including the example-specific objective functions, design parameters, and constraints utilized.

An estimate of the optimal design solution can be found through any preferred optimization strategy applied to Equation 1 to determine the actuation and activation parameters (within the physical bounds) that minimizes the difference between the deformed tile shape predicted by the forward problem and the target shape. Both standard gradient-based and non-gradient-based optimization strategies were utilized in the present study, with specific details provided in the Examples Section. As noted, specific focuses of the development were the shape difference metric and the parameterization strategy, which are discussed in more detail in the following.

Shape Difference Metric

There are multiple methods of shape description that can be used to quantify the difference between two shapes. In general, shape descriptors are separated into two categories: region-based shape descriptors (Lu and Sajjanhar 1999; Zhang and Lu 2004; Veltkamp 2001), which calculate the descriptor based on the entire volume of a shape, and contour-based shape descriptors (Veltkamp 2001), which calculate the descriptor based solely on the contour (or boundary) of the shape. Generally, region-based shape descriptors are not well suited for this type of application and so only contour-based descriptors were considered. Specifically, a sub-category of contour-based shape descriptors, correspondence-based shape descriptors, were considered.

One relatively intuitive correspondence-based approach is to project the target shape onto the initial tile shape (i.e., flat tile) to establish a point-to-point correspondence, and then measure the

difference between the location of the surface points on the target shape and the deformed location of the surface points estimated for a given design solution for all of these now corresponding points. Specifically for this work, a projection-based metric for a discretized tile surface was defined as:

$$PM_d = \sum_{i=1}^{N_C} \parallel \vec{x}_{Si} - \vec{x}_{Fi} \parallel, \tag{2}$$

where $\vec{x}_{Si}$ and $\vec{x}_{Fi}$ are the spatial coordinates on the target shape and deformed tile shape from the design estimate, respectively, for the i^{th} point in the correspondence set, N_C is the number of points in the point-to-point correspondence, and $\| \cdot \|$ is the Euclidean distance. Other similar approaches that first form a set of corresponding points between a target shape and an estimated morphed structure shape have been used in similar design applications (Lu and Kota 2003). However, these approaches can potentially limit the design space as they conceptually change the design problem to matching a desired displacement of certain points rather than a more general shape. Furthermore, the projection strategy considered here to form the correspondence is only applicable to target shapes with non-overlapping regions so that a one-to-one correspondence is formed. Alternatively, the Hausdorff distance and similar variants have been developed to quantify the difference between two shapes in a more general sense and with no limitation on the type of shapes being compared (Veltkamp 2001; Huttenlocher et al. 1993).

Assuming the shapes are discretized, the Hausdorff distance is a point-to-point matching that finds the maximum closest pairing between all the points on each shape. The Hausdorff distance between two shapes discretized into two collections of points S_1 and S_2 is defined as:

$$H_d(S_1, S_2) = \max(D(S_1, S_2), D(S_2, S_1)), \tag{3}$$

$$\text{where: } D(S_1, S_2) = \max_{\vec{x}_1 \in S_1} \min_{\vec{x}_2 \in S_2} \parallel \vec{x}_1 - \vec{x}_2 \parallel, \tag{4}$$

$\vec{x}_1$ is the collection of points in shape S_1, $\vec{x}_2$ is the collection of point in shape S_2, and again $\| \cdot \|$ is the Euclidean distance. A visual representation of $D(S_1, S_2)$ and $D(S_1, S_2)$ can be seen in Figure

2. An important note is that this Standard Hausdorff distance defined by Equation 3 can suffer from over-sensitivity to outliers, which can be expected as the Hausdorff distance is analogous to a L_∞ norm. To address these issues with the Hausdorff distance several modified versions have been developed and explored (Dubuisson and Jain 1994). For the present study the best performing modification in (Dubuisson and Jain 1994) was also considered alongside the Standard Hausdorff distance and the projection-based distance which can be defined as:

$$MH_d(S_1, S_2) = \max(M(S_1, S_2), M(S_2, S_1)) \tag{5}$$

$$\text{where: } M(S_1, S_2) = \frac{1}{N_1} \sum_{i=1}^{N_1} \min_{\vec{x}_2 \in S_2} \parallel \vec{x}_1 i - \vec{x}_2 \parallel, \tag{6}$$

N_1 is the number of points on shape S_1, $\vec{x}_1 i$ is the i^{th} point in $\vec{x}_1$, and N_2 is the number of points on shape S_2. This Modified Hausdorff distance is analogous to an L_1 norm and ensures that every point on each shape contributes to the distance metric.

Actuation and Activation Parameterization

When considering the computational design of a smart material structure such as the proposed SMP building tile, there are many methods available to activate and actuate the structure to achieve the desired behavior. Generally, in similar applications the entirety of the smart material is activated. However, additional functionality can be achieved through a mixture of smart material and a passive material, such as in (Peraza-Hernandez et al. 2013) which considered a Shape Memory Alloy (SMA) mesh binded to a passive material to achieve a self-folding structure. Alternatively, others have considered partial (or localized) smart material activation to increase functionality (Wang and Brigham 2012). As the activation process was not included in the system model for the work herein, there is no difference conceptually in the optimal design procedure whether the intention is to use localized activation or to combine active and passive materials. In both cases, the objective of the activation portion of the optimal design are the same, which is to define the distribution (i.e., size and location) of the regions of the structure that would have the activated (i.e., soft) material properties.

For any inverse problem where the objective is to obtain the material property distribution, there are many different ways to parameterize the unknowns. The main concern with the parameterization is often the trade-off between generality (i.e., being able to capture any possible distribution) and computational expense. The more general the parameterization the higher the computational expense of the problem. For example, finite element-type discretizations of a material property distribution (Wang et al. 2015), for which every node or element of a mesh can have a different property, have a high degree of general applicability. However, the large number of unknowns in a mesh description can substantially increase computational expense and may require some kind of regularization or other additional consideration to address ill-posedness. Alternatively, many lower-dimensional parameterizations have been considered to reduce computational expense and avoid ill-posedness, such as the use of radial basis functions (Ahmadpoor et al. 2016). The challenge with lowering the dimension of the parameterization is that it is often problem-dependent and best used when some *a priori* information is available or can be estimated regarding the expected type of spatial distribution.

In order to balance computational cost with generality for this specific application, the distribution of activated material was parameterized into a fixed number of activated regions, assuming the material would be activated uniformly through the thickness. The number of regions was chosen to be sufficiently large to allow for complex solutions (e.g., many disconnected activated regions), but the regions could overlap to allow for simple solutions as well (e.g., a single local activated region). Furthermore, a threshold was set so that any small gaps between activated or inactivated material regions would be removed to improve practicality of the design solutions. Thus, the material distribution was defined by m discrete activated material sections centered at variable planar locations, $\{d_j\}_{j=1}^{m}$, along the tile with variable widths/diameters, $\{l_j\}_{j=1}^{m}$. An important note is that this parameterization of the material activation is expected to lead to non-unique solutions in terms of the parameters, even for cases where there is one optimal distribution of material properties. However, this non-uniqueness was not a concern, since the distribution and not the parameters themselves is the important outcome, and uniqueness in optimal design problems is generally not

critical. The actuation was chosen to be implemented through variable applied pressure and a series of n discrete actuators at variable planar locations, $\{c_i\}_{i=1}^{n}$, and with variable horizontal and vertical prescribed displacements, $\{u_i\}_{i=1}^{n}$ and $\{w_i\}_{i=1}^{n}$, respectively. Figure 3 shows a two-dimensional (2D) schematic of the tile with an applied pressure P, n discrete actuators, and m discrete activated zones for a maximum of $3n + 2m + 1$ potential design variables to be determined.

RESULTS AND DISCUSSION

Several numerical case studies of the design of a smart material shape changing tile were considered to evaluate the capability of the shape-based optimal design strategy presented to achieve nontrivial design solutions and examine any potential benefits or limitations for the various component options discussed. In all examples the conceptual shape-changing tile was taken to be 10.16 cm-by-10.16 cm (4 in-by-4 in) with a thickness of 0.25 cm (0.1 in) and the activated and inactivated mechanical material properties were based upon those for a standard shape memory polymer (SMP) (Beblo et al. 2010). Although it is not expected that such a material would be suitable for architectural applications without further development/modification, the shape memory and large recoverable strain capabilities of SMP (Leng et al. 2011) would be significantly beneficial for the proposed concept of a shape changing building skin tile. Therefore, SMP was chosen as the exemplar smart material for the development of this concept. The material was assumed to be an isotropic Neo-Hookean hyperelastic material model with activated and inactivated Young's moduli of 2.4 MPa and 1034 MPa, respectively, and a constant Poisson's ratio of 0.45. The process to change the shape (i.e., deform) the tile was assumed to be quasi-static. As previously noted, the material was assumed to be activated instantaneously so that regions of the tile were either activated or inactivated completely, and it was further assumed that all activation of material occurred prior to the application of any actuation. A final important consideration not yet mentioned for the design of this type of smart material shape-changing structure is to ensure that the design solution does not damage the structure. Although a constraint could be included in the design optimization problem to prevent solutions that damage the material (Wang and Brigham 2012), preliminary tests showed this to be unnecessary for the case studies considered. However, the final design solutions were still

checked to ensure no damage of the material would occur by confirming the maximum principal strain did not exceed damage limits anywhere of 30% for inactivated material or 400% for activated material.

In addition to the capability to identify nontrivial design solutions to complex problems, a primary benefit of a computational design approach such as that proposed is the generalisability in contrast to more traditional design strategies. Therefore, the focus of the test cases used to evaluate the capability of this approach was not just to show that the approach could be successfully applied to the morphing façade tile concept, but to also show the range of applicability without the need to fundamentally change the solution strategy. In particular, the examples chosen focused on the capability to identify relatively high-quality design solution regardless of the fundamental nature of the topology (assuming a continuous surface) and the degree of spatial variability of the desired surface shape, while also including a range of actuation and activation types and constraints, and being able to incorporate additional design objectives (not just a target shape).

To explore variations in the fundamental topology of the target shape for the morphing structure, two classes of target shapes were considered: (1) convex surfaces (for which the projection strategy for the design objective would be applicable) and (2) non-convex surfaces. In addition, within each of these classes one target shape was considered with a "smooth" spatial variation and another non-smooth target shape with "sharp" changes in the surface was considered to see if this aspect also had an effect on the solution capability. The majority of the test cases considered one direction of spatial variability for the target shape (i.e., two-dimensional target shapes). However, to also show that the design approach generalizes to a higher degree of spatial variability, one additional test case was considered for a target shape with two directions of spatial variability (i.e., a three dimensional target shape).

Throughout the test cases, the independence of the solution strategy with respect to the design parameters (i.e., activation and actuation) is shown by changing both the number of discrete design parameters and the physical property these parameters define. Initially, the actuation of the morphing structure is fixed and the design parameters only relate to the number and location of

actuators. Then, the capability of the morphing structure to have variable actuation was included, and these new design parameters defined the location and size of the activated material. The case of variable actuation also facilitated the consideration of additional design problem objectives (in addition to the target shape), as energy cost would be a potentially important design component for a morphing structure and amount of material activated can often represent the largest energy cost. Thus, the design approach was modified to account for multiple objectives, the target shape and the energy cost, and the capability of the computational approach to elucidate the range of design solutions with respect to multiple objectives and their corresponding trade-off is shown.

Table 1 shows the design cases considered in the order they appear and their corresponding topology classification, the design parameters to be determined, and the design objectives considered (as well as whether single or multi-objective design). More details of the case studies will be given in their respective sections.

Capability of a Shape-Based Objectives for Optimal Design

In Cases 1 and 2 the capability of the correspondence-based shape difference metrics as objective functions to accurately match a target shape were investigated. For both of these cases, the tile was assumed to be fully activated (i.e., the only optimization parameters to be considered were the mechanical actuation variables) to simplify the design solution space, so that the capability of the various objective functions could be more easily compared. Full activation was considered to focus on the design objective functions, rather than comparing the capabilities of local to global activation. Furthermore, energy cost was ignored for these first tests (i.e., not included in the optimization), since the activation energy is typically the primary energy cost and was not varying for these tests.

For both Cases 1 and 2, a constrained gradient-based interior point algorithm was used to solve Equation 1 by minimizing $C\left(S_T, S_F(\vec{u})\right)$ (removing the energy term from Equation 1). For each numerical example, the gradient-based optimization was repeated with 10 randomly generated initial guesses and the solution was taken to be the result with the lowest respective objective function value. The optimization stopping criteria was set to be when the change in objective

function between iterations fell below the tolerance value of 10^{-6}. Starting with one actuator, the number of actuators for the design was increased by one and the optimization repeated until the shape matching capability did not noticeably improve (i.e., convergence was achieved in terms of the number of actuators). This type of optimization was done for simplicity since the parameter for the number of actuators is an integer, while the remaining design parameters are continuous real numbers. Each of the correspondence-based objective functions defined in Section 3, the Standard Hausdorff distance, the Modified Hausdorff distance, and the projection-based distance, were used in turn as the objective function for the optimization process. In order to have a fair comparison between each of the potential design solutions, regardless of the objective function used in the optimization process, the Standard Hausdorff distance and Modified Hausdorff distance were calculated for the final designed tile shapes in comparison to the target shapes. The design problem was constrained to be two-dimensional by assuming both the activation and actuation would be constant in one planar direction. Additionally, for Cases 1 and 2 the two end faces of the tile that were parallel to the direction of constant activation and actuation were taken to be fixed with zero displacement in all directions (as shown in Figure 3), while all other faces were free to deform due to the actuation detailed in Section 3.

Convex Target Shapes

Figure 4 shows the two target shapes considered in this case, an “overhang" shape (Target Shape 1) and a unidirectional sin-wave (Target Shape 2) for this case. Both shapes were based upon work in (Zupan et al. 2018), which detailed the self-shading performance of these shapes in a similar application for a building skin. Both target shapes are convex with one direction of spatial variability. Target Shape 1 had a flat (i.e., undeformed) cross-section for half of the tile, and the other half had a cross-section defined by a single sin wave with amplitude 4.57 *cm* and a period of 5.08 *cm*, due to the discontinuity this shape is considered “non-smooth". Target Shape 2 was defined by a sin wave cross-section with amplitude 2.74 *cm* and a period of 5.08 *cm*, this shape is considered “smooth".

Figure 5 shows the Standard and Modified Hausdorff distances for the final design shapes

obtained from optimizing with respect to each of the correspondence-based objective functions with one through five discrete actuators for Target Shapes 1. No sufficiently accurate solution could be found for a one actuator design, which is consistent with intuition. However, all design solutions that utilized two or more actuators for Target Shape 1 resulted in Standard and Modified Hausdorff distances less than 10% the length increase (2.08 *cm*) of the tile, with only the exception of the four actuator case using the Standard Hausdorff objective function that had a slightly higher error. In other words, the design solution converged at two actuators for Target Shape 1. The shape matching for Target Shape 1 when minimizing with respect to all three objective functions can be seen in Figure 6, which shows the final deformed shape and the design solution (i.e., actuator placement and pressure) corresponding to each objective function. Clearly, designs that can accurately match the target shape were able to be obtained when they existed, regardless of the specific shape-based objective function utilized in this case. The convergence at two actuators is expected based on the key features of the shape (i.e., one actuator to hold the first half of the tile in place and a second actuator to define the height of the "overhang"). Also of note, there are fluctuations in the Standard and Modified Hausdorff distances for the final design shapes, most notably for the solutions obtained by minimizing the Standard Hausdorff distance. The larger fluctuations in the solutions, imply that the Standard Hausdorff Distance creates a more complex solution space that is more difficult for an optimization algorithm to traverse (i.e., more local minima exist in comparison to the other objective functions).

The results for Target Shape 2 were similar to those for Target Shape 1, but accurate design solutions were not able to be obtained until at least 3 actuators were utilized (Figure 7). The shape matching for Target Shape 2 when minimizing with respect to all three objective functions can be seen in Figure 8, which shows the final deformed shape and the design solution corresponding to each objective function. A main difference in the results for Target Shape 2 is that an odd number of actuators were necessary to accurately match the desired shape, with even numbers of actuators resulting in errors as high as 300% more than when using an odd number of actuators. This is due to the need for an odd number of actuators to be able to match the key features of a symmetric

shape, by placing one actuator at the line of symmetry and an equal number on each side of the line of symmetry. Consistent with the results from Target Shape 1, the Standard Hausdorff distance objective function resulted in a more challenging optimization problem and led to the identification of inaccurate design solutions in terms of the shape matching for some cases of Target Shape 2.

An important note is there are design solutions that have nearly identical actuator placements and deformations, but substantially different applied pressure values for both Target Shapes 1 and 2, as seen in Figures 6 and 8. This could be interpreted as the pressure variable being a superfluous variable in the design of the shape changing mechanisms and should likely be removed from the system if implemented for these cases. However, as will be shown in the following, the ability to control an applied pressure became significant for more complicated target shapes and when utilizing localized activation.

Non-Convex Target Shapes

Figure 9 shows the two target shapes considered in this case, a boxcar function (Target Shape 3) and a distorted sin-wave (Target Shape 4), for this case. Both target shapes are non-convex with one direction of spatial variability. Target Shape 3 was a centered boxcar function with a width of 5.08 *cm* and a height of 2.54 *cm*, due to the discontinuities in the shape it is considered "non-smooth". Target Shape 4 was a centered sin-wave with an amplitude of 2.62 *cm* and a period of 10.16 *cm*, which was rotated 75° about the out-of-plane axis, this shape is considered "smooth". As projection is not applicable for these shapes, only the Standard and Modified Hausdorff distances were used as objective functions within the design optimization procedure for this case. Additionally, in these examples the number of actuators was incremented from one to seven, due to the increased target shape complexity.

Figures 10 and 11 show the Standard and Modified Hausdorff distances for the final design shapes obtained from optimizing with respect to those same two applicable correspondence-based objective functions with one through seven discrete actuators for Target Shapes 3 and 4, respectively. Even with the substantial increase in target shape complexity, solutions that clearly matched Target Shapes 3 and 4 could be found. The sufficiency of the design solutions can be visually confirmed

through Figures 12 and 13, which show the final deformed shapes and design solutions corresponding to each objective function. Even though the optimization process typically converged to a design solution with a higher error than the prior set of examples (e.g., error values of approximately 10% of the length change of the tile), the optimization process using the Modified Hausdorff distance led to design solutions that matched both of the complex target shapes accurately. Alternatively, the limitation of the Standard Hausdorff distance that resulted in less consistent optimization was even more significant, with the corresponding design solutions for Target Shapes 3 and 4 being substantially less accurate, both quantitatively and visually.

Regarding the design variables, as expected the optimal design process revealed that this more complex second set of target shapes required more actuators (four or five) in comparison to the prior example set (two or three actuators) to accurately match the desired shapes. Additionally, in contrast to the previous set of examples, the pressure design variable was an important variable to the design, and consistent pressure values were identified for the design solutions that accurately matched the target shapes.

Locally Activated Shape Changing Tile

After establishing the capabilities of the shape difference metrics, Case 3 focused on the use of localized material activation for the design of a smart material shape-changing structure. To investigate the optimal design problem now with localized material activation rather than full activation, a subset of the target shapes from both of the prior test sets were considered: Target Shape 2 (unidirectional sin-wave, Figure 4(b)) and Target Shape 4 (distorted sin-wave, Figure 9(b)).

To contrast with the previous results with full activation in terms of shape matching accuracy, an optimization process similar to the previous two cases (a constrained gradient-based interior point algorithm) was utilized to find design solutions. The localized activation was implemented as described in Section 3. Due to prior results shower higher accuracy, the Modified Hausdorff distance was the only shape metric considered in this case.

Figures 14(a) and 14(b) show the value of the Modified Hausdorff distance for the final design shapes obtained from optimizing with respect to the Modified Hausdorff distance with one through

four discrete actuators for Target Shapes 2 and 4 for both localized activation and full activation (i.e., the same as those shown in Figures 7 and 11). Specifically, in Figure 14(a) it can be seen that, with the exception of one actuator, the optimization procedure that included localized activation found design solutions that resulted in lower Modified Hausdorff distance values (i.e., better shape matching) for Target Shape 2 than when using full activation. Similarly considering Target Shape 4 (Figure 14(b)), the optimal designs utilizing localized material activation resulted in lower Modified Hausdorff distance values for every design case. The design solutions using localized activation were even capable of improving the shape matching for Target Shape 4 using less actuators (e.g., one actuator with localized activation was more accurate than four actuators with full activation). This shows that the design strategy was able to determine these non-intuitive (based on previous results) solutions when including localized activation. Thus, there is clear benefit to the use of localized activation to achieve improved shape matching of a smart material morphing structure. Moreover, the use of less actuators to achieve a more accurate shape indicates that the use of localized activation is not only beneficial for shape matching purposes but also does so with a lower energy cost in terms of both thermal activation and mechanical actuation.

Target Shape with Two Directions of Spatial Variability

For this group of numerical case studies, the same approach for the design optimization as the first group of tests was used (interior point algorithm minimizing shape difference) with the Modified Hausdorff distance used as the objective function. The same concept of variable parameterization was used as for the previous examples, however the discrete actuators were removed from the design space in order to reduce the complexity of the design space (i.e., the only actuation was the applied pressure). The activation was defined by a set of circular regions on the 3D tile, activating uniformly through the thickness as before, with controllable center locations and diameters. Differing from the previous three groups of tests (which had 2 fixed edge faces and 2 free edge faces), all four outer edge faces were fixed to have zero displacement in all directions and the target shape considered has two directions of spatial variability.

Figure 15 shows the target shape, a boxcar function extended to three dimensions. The boxcar

portion of the target shape had a height of 1.27 cm and was centered on the lines $x = 1.27$ cm and $y = 0$ cm with a width of 2.54 cm and a length of 7.62 cm. This target shape was chosen to be similar to an overhang shape (a common shading device).

Figure 15 shows the location of the activated material for the final design solution. These activated regions are concentrated over the location of the boxcar portion of the target shape, which is consistent with what would be expected given the constraints on the design problem. The Modified Hausdorff distance between the deformed model surface and the 3D target shape for this design solution was 0.20 cm. A plot of a cross-section (taken at $y = 0$ cm) of the target shape and the deformed model surface of the design solution is shown in Figure 17. In this case the design optimization was not able to reach a solution with the sharp features of the 3D target shape. This is due to only using a uniform pressure which will always result in a smooth, continuous solution. However, the Modified Hausdorff distance of 0.20 cm can be considered a small value, particularly in comparison to the prior examples in Section 4, which has Modified Hausdorff distance values of 0.20 cm for two or more actuators. Furthermore, although the deformed tile is observably different than the 3D target shape, this design solution still resembles an overhang, which was the goal of choosing the target shape in the first place.

Multi-Objective Design - Shape Difference and Energy Cost

When utilizing local activation, the energy cost to change the structure's shape varies far more significantly depending upon the design than for the previous cases. Therefore, to explore the capability to design utilizing additional objectives (in addition to the shape targeting) energy was included as an objective in Case 5.

For this multi-objective case a controlled, elitist genetic algorithm (Guide 1998) was used to solve Equation 1 by simultaneously minimizing both $C(S_T, S_F(\vec{u}))$ and $E(\vec{u}, \vec{\gamma})$ to determine potential design solutions. The initial population was set to be 200 and the stopping criteria was set as either a maximum number of generations of $200 * N_D$ (where N_D is the number of design variables) or when the objective function difference between iterations fell below a tolerance of 10^{-4}). The result of the multi-objective optimization for each trial was the Pareto front set of

solutions. The Pareto front includes all of the “best" potential design solutions within the limit of the population size that have a lower value for at least one of the separate objective functions in comparison to any other solution estimate seen throughout the optimization process. This Pareto front is particularly useful to analyze the trade-off between the two objectives, shape matching accuracy and energy cost. Similar to the first three cases of numerical tests the design problem was again constrained to be two dimensional and have the same boundary conditions.

As the Modified Hausdorff distance was universally applicable and led to substantially more consistent design solutions compared to the other objectives considered, this was the only shape-based objective function used for the following case. Based on the example of a thermally activated SMP, the energy required to morph the smart material tile in this application could be quantified from the design pressure, mechanical actuation, and material activation as follows:

$$E = \int_{\Gamma} P(-\vec{n} \cdot \vec{u}) d\Gamma + \sum_{i=1}^{n} \vec{F}_i \vec{u}_i + c_p \rho V_a \Delta T, \tag{7}$$

$\vec{n}$ is the unit outward normal to the tile surface where pressure was applied, Γ, $\vec{u}$ is the displacement vector, $\vec{F}_i$ is the resultant force vector needed to displace the i^{th} mechanical actuator by $\vec{u}_i$, c_p is the specific heat of the SMP (taken as $c_p = 2009 \frac{J}{kg-K}$), ρ is the density of the SMP (taken as $\rho = 35.98 \frac{kg}{m^3}$), ΔT is the temperature change required to activate the material, and V_a is the volume of the tile that is activated (determined based on the activated zone parameterization defined in Section 3). As noted previously, the activation process was not considered within this study. Therefore, to quantify the energy to activate the material, it was assumed that the activated zones would have to be heated from room temperature ($18°C$) to the SMP activation temperature of $25°C$, resulting in a fixed temperature change for the activated zones of $\Delta T = 7°C$.

The target shapes considered for Case 5 were again a subset of the previous shapes considered, specifically Taget Shapes 2 (Figure 4b) and 4 (Figure 9b). The design strategy was capable of finding Pareto fronts for both of the target shapes considered in Case 5. Figure 18 shows the composite Pareto fronts in terms of the total energy cost and final Modified Hausdorff distance

for the potential designs obtained from the multi-objective optimization for Target Shapes 2 and 4. These composite Pareto fronts were constructed from the final populations of potential design solutions for each case of one through five actuators. One method for choosing the preferred solution (i.e., single optimal solution) from a Pareto front is to select the solution that is nearest to the origin along the front. The two optimal design solutions (one for each Target Shape) that were nearest to the Pareto front origin are shown in terms of the deformed shapes, actuator placements, and activated zones in Figures 19 and 20.

Both Pareto fronts determined from the design strategy corresponding to Target Shape 2 and 4 show a distinct point of diminishing returns in terms of both objectives, with each Pareto front having a clear L-shape. For example, for Target 2 in order to reduce the energy cost by 30% from the optimal solution on the L-shaped curve the accuracy of the shape matching must be reduced by 173%. Similarly, in order to improve the shape matching accuracy by 4% from the optimal solution, the energy cost increases by 17%. To examine the design solutions further, the relative contribution of the mechanical actuation and the material activation to the morphing energy cost was examined for each case. It was found that the material activation energy cost was significantly greater than the mechanical actuation energy cost in all cases, but the extent of which was dependent on the number of actuators utilized for the design. Specifically, when one actuator was utilized the thermal energy cost was greater than 90% of the total energy cost while it was as low as 60% of the total energy cost while utilizing five actuators. Thus, there were at times highly non-intuitive outcomes in balancing the number of actuators, total energy cost, and shape accuracy that the design strategy was able to determine. Further related to energy efficiency, Figures 19 and 20 show that even though 20 separate activated zones ($m = 20$) could be utilized, the push for efficiency naturally led to smooth (i.e., a small number of continuous activated regions rather than a large number of small activated zones) results, and in affect, regularized the solution (eliminating the need for regularization of the parameterization). Looking more closely at the Pareto front corresponding to Target Shape 2 (Figure 18(a)), the solutions clustered around the point nearest the Pareto front origin generally utilized three or five actuators, while the solutions with higher

Modified Hausdorff distance values and lower energy cost utilized a mixture of one, two, and four actuators. Considering the Pareto front corresponding to Target Shape 4 (Figure 18(b)), it was found that all solutions with a Modified Hausdorff distance below 0.19 *cm* utilized four actuators, while the remainder utilized two actuators. Again, the fluctuations in the solutions are non-intuitive in comparison to the previous single objective optimization and indicate the necessity of a design approach, such as that presented, for maximum shape matching and energy cost benefits.

CONCLUSIONS

The development and evaluation of a computational approach for optimal design of a smart material shape changing building skin tile was presented. This approach was evaluated through numerical examples that considered the capability of the computational procedure while utilizing various shape-based objectives and design variable parameterizations to accurately match target shapes with a variety of features (convex/non-convex, smooth/non-smooth, and one/two directions of spatial variability). The results from the design approach indicated that the computational approach utilizing the shape-based objective functions can result in mechanisms of morphing that lead to accurate deformed shapes in comparison to various target shapes. Of the shape metrics considered, the Modified Hausdorff distance was shown to be preferable because the computational approach utilizing the Modified Hausdorff distance resulted in the most consistently accurate shape matching. Additionally, the computational approach utilizing the Modified Hausdorff distance was applicable to any shape, even non-convex target shapes, while retaining acceptable deformed shape accuracy. The results from the design approach also indicated that the use of localized material activation for the design of a smart material shape changing structure of the type considered here can lead to higher accuracy in matching target shapes (i.e., better functionality) than a design that only has the capability to activate the entire structure. However, the design space for the system considered had a significant trade-off between shape matching accuracy and energy cost. Yet, the ability to use localized activation for the design was shown to require considerably less energy to perform the shape change and to require less actuation devices, potentially benefiting implementation considerably.

One limitation of this approach is the computational expense, particularly when using the Standard or Modified Hausdorff distances. This is due to the sensitivity of the two metrics to outliers (albeit the Standard Hausdorff distance is much more sensitive). The computational expense could be reduced in various ways including developing and using differentiable forms of the Hausdorff metrics, modifying the Modified Hausdorff distance to further reduce sensitivity to outliers, and implementing a faster forward model approach (mesh-free analysis opposed to standard finite element analysis).

ACKNOWLEDGMENTS

The authors gratefully acknowledge the financial support of the National Science Foundation through Award No. 1536797.

REFERENCES

Ahmadpoor, M., Notghi, B., and Brigham, J. C. (2016). "A generalized iterative approach to improve reduced-order model accuracy for inverse problem applications." *Journal of Engineering Mechanics*, 142(5), 04016020.

Barrett, R. M. and Barrett, R. P. (2016). "Thermally adaptive building covering field test." *Procedia Engineering*, 145, 26–33.

Beblo, R., Gross, K., and Mauck Weiland, L. (2010). "Mechanical and curing properties of a styrene-based shape memory polymer." *Journal of Intelligent Material Systems and Structures*, 21(7), 677–683.

Bridgens, B. (2018). "Hygromorphic tile concept, <https://blogs.ncl.ac.uk/responsive-materials>.

Cilento, K. (2012). "Al bahar towers responsive facade/aedas." *ArchDaily,'September*, 5.

Clifford, D. (2019). "Cactus tile concept, <http://cmubiologic.weebly.com/cactus-tile.html>.

Dewidar, Y., Mohamed, N., and Ashour, Y. (2013). "Living skins: A new concept of self active building envelope regulating systems." *Advancing the Green Agenda; Technology, Practices and Policies Conference–BUID*, 1–8.

Dubuisson, M.-P. and Jain, A. K. (1994). "A modified hausdorff distance for object matching." *Pattern Recognition, 1994. Vol. 1-Conference A: Computer Vision & Image Processing., Proceedings of the 12th IAPR International Conference on*, Vol. 1, IEEE, 566–568.

Guide, M. U. (1998). "The mathworks." *Inc., Natick, MA*, 5, 333.

Holstov, A., Bridgens, B., and Farmer, G. (2015). "Hygromorphic materials for sustainable responsive architecture." *Construction and Building Materials*, 98, 570–582.

Huttenlocher, D. P., Klanderman, G. A., and Rucklidge, W. J. (1993). "Comparing images using the hausdorff distance." *IEEE Transactions on pattern analysis and machine intelligence*, 15(9), 850–863.

Jani, J. M., Leary, M., Subic, A., and Gibson, M. A. (2014). "A review of shape memory alloy research, applications and opportunities." *Materials & Design (1980-2015)*, 56, 1078–1113.

Lampert, C. M. (2004). "Chromogenic smart materials." *Materials today*, 7(3), 28–35.

Leng, J., Lan, X., Liu, Y., and Du, S. (2011). "Shape-memory polymers and their composites: stimulus methods and applications." *Progress in Materials Science*, 56(7), 1077–1135.

Liu, Y., Du, H., Liu, L., and Leng, J. (2014). "Shape memory polymers and their composites in aerospace applications: a review." *Smart Materials and Structures*, 23(2), 023001.

Lu, G. and Sajjanhar, A. (1999). "Region-based shape representation and similarity measure suitable for content-based image retrieval." *Multimedia Systems*, 7(2), 165–174.

Lu, K.-J. and Kota, S. (2003). "Design of compliant mechanisms for morphing structural shapes." *Journal of intelligent material systems and structures*, 14(6), 379–391.

Mather, P. T., Luo, X., and Rousseau, I. A. (2009). "Shape memory polymer research." *Annual Review of Materials Research*, 39, 445–471.

Mohaghegh Motlagh, S. A. (2014). "An investigation in structural shape morphing by modulus variation." Ph.D. thesis, University of Pittsburgh, University of Pittsburgh.

Molinari, G., Quack, M., Arrieta, A. F., Morari, M., and Ermanni, P. (2015). "Design, realization and structural testing of a compliant adaptable wing." *Smart Materials and Structures*, 24(10), 105027.

Namgoong, H., Crossley, W., and Lyrintzis, A. (2006). "Morphing airfoil design for minimum aerodynamic drag and actuation energy including aerodynamic work." *47th AIAA/ASME/ASCE/AHS/ASC Structures, Structural Dynamics, and Materials Conference 14th AIAA/ASME/AHS Adaptive Structures Conference 7th*, 2041.

Otsuka, K. and Wayman, C. M. (1999). *Shape memory materials*. Cambridge university press.

Peraza-Hernandez, E., Hartl, D., and Malak, R. (2013). "Simulation-based design of a self-folding smart material system." *ASME 2013 International Design Engineering Technical Conferences and Computers and Information in Engineering Conference*, American Society of Mechanical Engineers, V06BT07A045–V06BT07A045.

Prock, B., Weisshaar, T., and Crossley, W. (2002). "Morphing airfoil shape change optimization with minimum actuator energy as an objective." *9th AIAA/ISSMO Symposium on Multidisciplinary Analysis and Optimization*, 5401.

618 Shameri, M., Alghoul, M., Sopian, K., Zain, M. F. M., and Elayeb, O. (2011). "Perspectives of
619 double skin façade systems in buildings and energy saving." *Renewable and Sustainable Energy*
620 *Reviews*, 15(3), 1468–1475.
621 Sun, J., Liu, Y., and Leng, J. (2015). "Mechanical properties of shape memory polymer composites
622 enhanced by elastic fibers and their application in variable stiffness morphing skins." *Journal of*
623 *Intelligent Material Systems and Structures*, 26(15), 2020–2027.
624 Veltkamp, R. C. (2001). "Shape matching: Similarity measures and algorithms." *Shape Modeling*
625 *and Applications, SMI 2001 International Conference on.*, IEEE, 188–197.
626 Wang, M., Dutta, D., Kim, K., and Brigham, J. C. (2015). "A computationally efficient approach
627 for inverse material characterization combining gappy pod with direct inversion." *Computer*
628 *Methods in Applied Mechanics and Engineering*, 286, 373–393.
629 Wang, S. and Brigham, J. C. (2012). "A computational framework for the optimal design of mor-
630 phing processes in locally activated smart material structures." *Smart Materials and Structures*,
631 21(10), 105016.
632 Woods, B. K. and Friswell, M. I. (2016). "Multi-objective geometry optimization of the fish bone
633 active camber morphing airfoil." *Journal of Intelligent Material Systems and Structures*, 27(6),
634 808–819.
635 Yu, K., Yin, W., Sun, S., Liu, Y., and Leng, J. (2009). "Design and analysis of morphing wing based
636 on smp composite." *Industrial and Commercial Applications of Smart Structures Technologies*
637 *2009*, Vol. 7290, International Society for Optics and Photonics, 72900S.
638 Zhang, D. and Lu, G. (2004). "Review of shape representation and description techniques." *Pattern*
639 *recognition*, 37(1), 1–19.
640 Zupan, R. J., Beblo, R. V., Clifford, D. T., Aggarwal, A., and Brigham, J. C. (2017). "Design
641 optimization of a self-shading smart material morphing building skin.
642 Zupan, R. J., Clifford, D., Beblo, R., and Brigham, J. (2018). "Numerical investigation of capabili-
643 ties for dynamic self-shading through shape changing building surface tiles." *Journal of Facade*
644 *Design and Engineering*, 6(1).

List of Tables

Case	Topology	Smoothness	Directions of Spatial Variability	Actuation	Activation	Objective(s)
1	Convex	Smooth and Non-smooth	One	Actuators and Pressure	Full	Shape Difference
2	Non-Convex	Smooth and Non-smooth	One	Actuators and Pressure	Full	Shape Difference
3	Convex and Non-convex	Smooth	One	Actuators and Pressure	Localized	Shape Difference
4	Non-convex	Non-smooth	Two	Pressure	Localized	Shape Difference
5	Convex and Non-convex	Smooth	One	Actuators and Pressure	Localized	Shape Difference and Energy

TABLE 1. Summary of the numerical cases considered in this work.

List of Figures

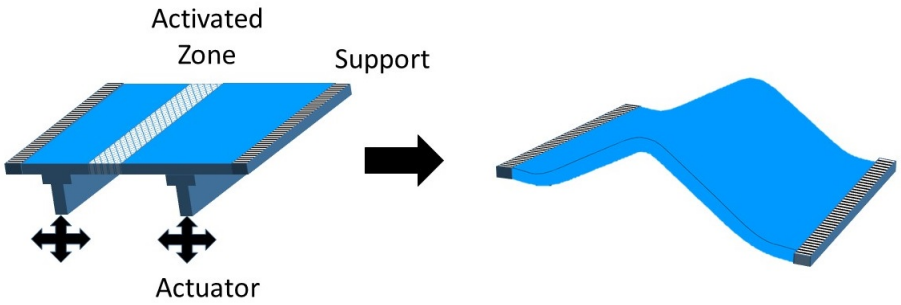

Fig. 1. Concept of a smart material being activated and mechanically actuated.

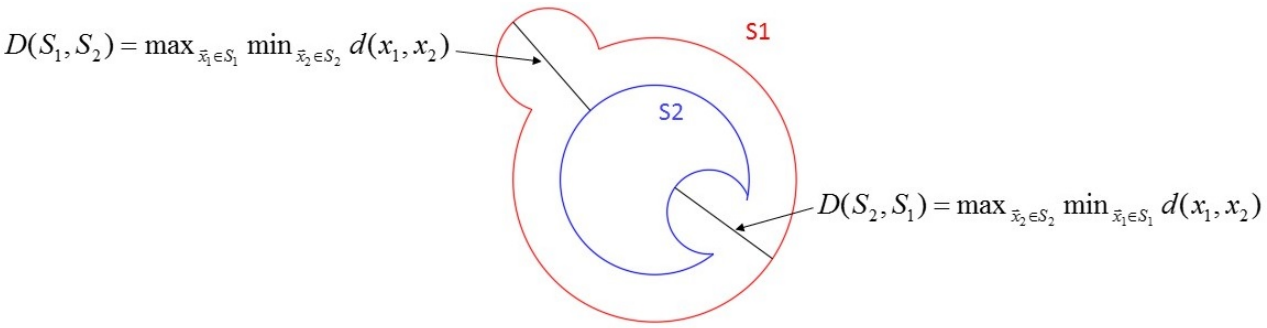

Fig. 2. Representation of the distances $D(S_1, S_2)$ and $D(S_2, S_1)$ used in Equation 4 for shapes S_1 and S_2

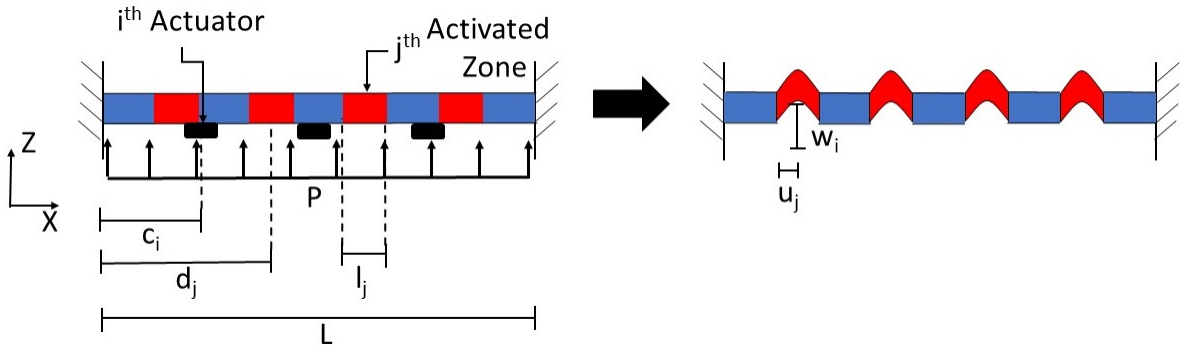

Fig. 3. Schematic of the tile concept in which applied pressure (P), a series of n discrete actuators at variable locations, and a set of m activation patches (red) at variable locations are used to deform the tile to achieve a given target shape.

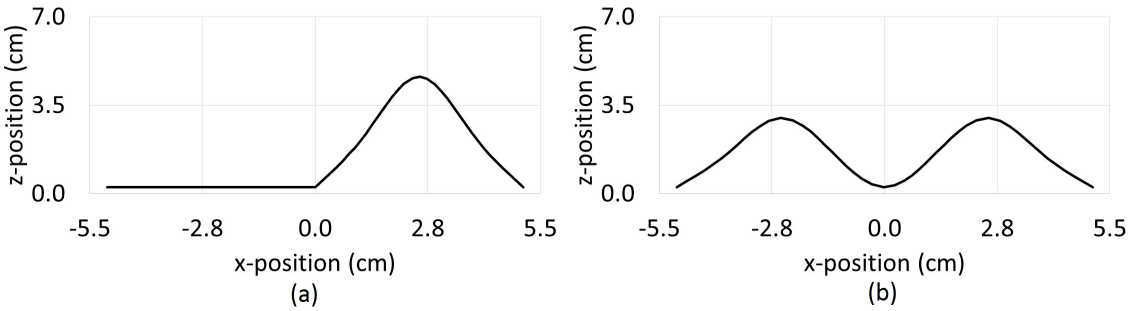

Fig. 4. The two target shapes considered in the convex group. (a) An “overhang" shape (Target Shape 1) and (b) a unidirectional sin-wave (Target Shape 2).

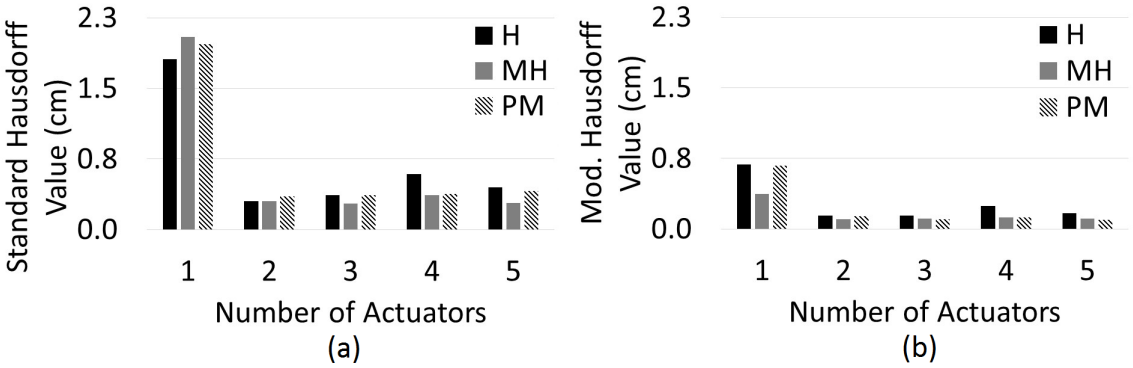

Fig. 5. (a) Standard Hausdorff distance value and (b) Modified Hausdorff distance for optimal designs using various numbers of actuators for design solutions minimizing with respect to the Standard Hausdorff, Modified Hausdorff, and projection-based distances for Target Shape 1.

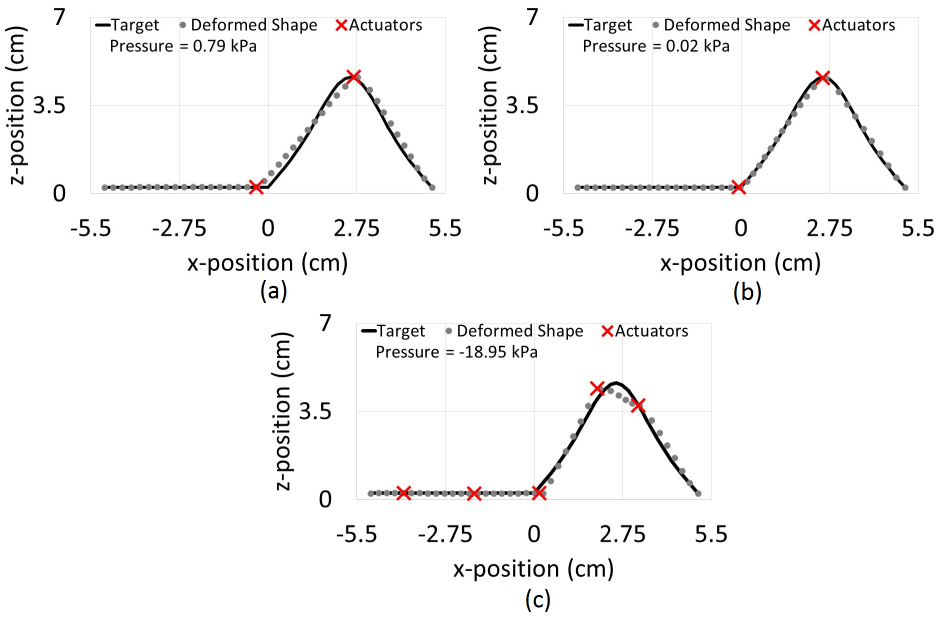

Fig. 6. The morphed tile shape for the “best" design solution, target shape, and actuator placement for the optimization using (a) the Standard Hausdorff distance, (b) the Modified Hausdorff distance, and (c) the projection-based distance for Target Shape 1.

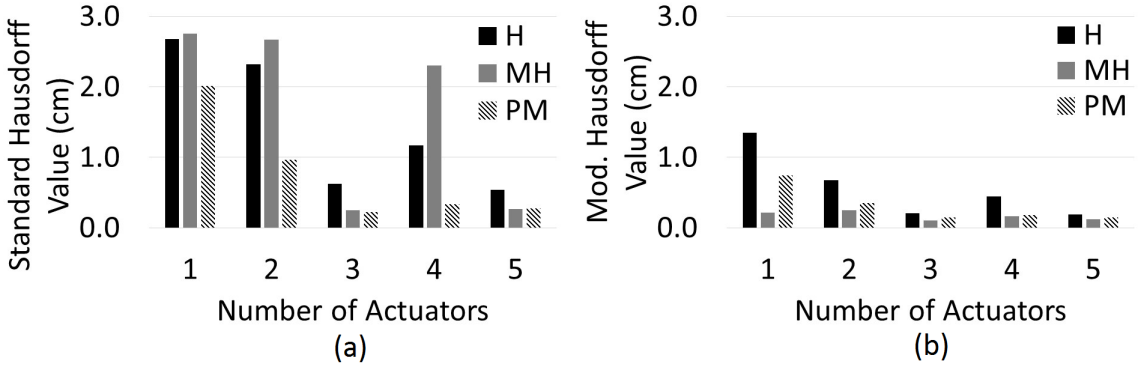

Fig. 7. (a) Standard Hausdorff distance value and (b) Modified Hausdorff distance for optimal designs using various numbers of actuators for design solutions minimizing with respect to the Standard Hausdorff, Modified Hausdorff, and projection-based distances for Target Shape 2.

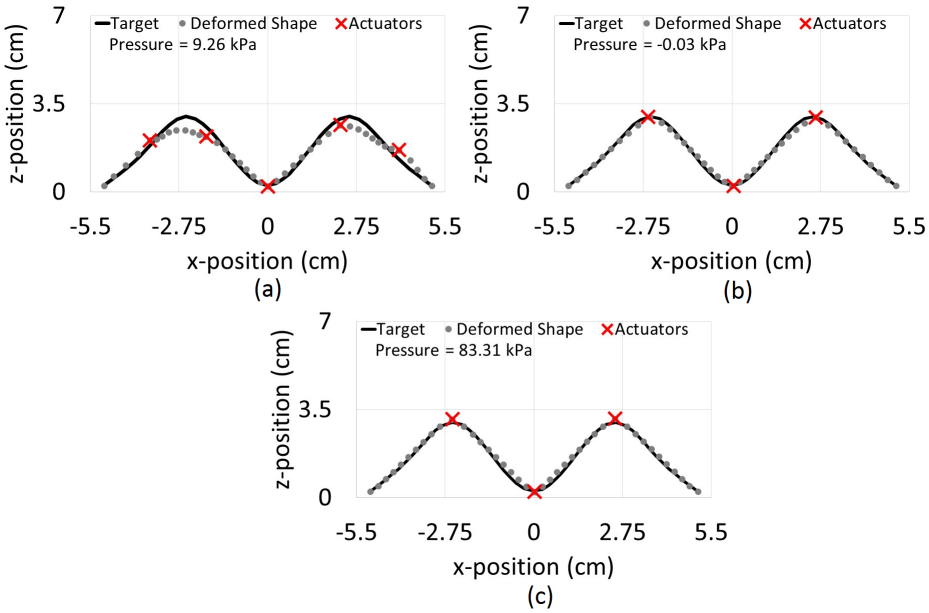

Fig. 8. The morphed tile shape for the “best" design solution, target shape, and actuator placement for the optimization using (a) the Standard Hausdorff distance, (b) the Modified Hausdorff distance, and (c) the projection-based distance for Target Shape 2.

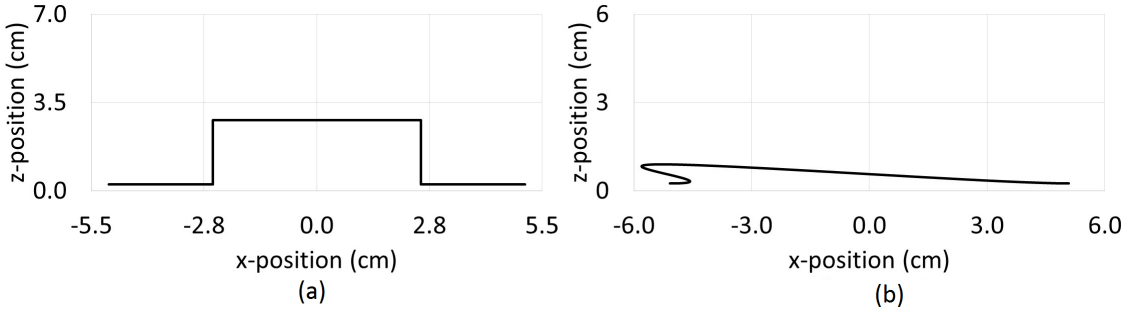

Fig. 9. The two target shapes considered in the non-convex group. (a) A boxcar function (Target Shape 3) and (b) a distorted sin-wave (Target Shape 4).

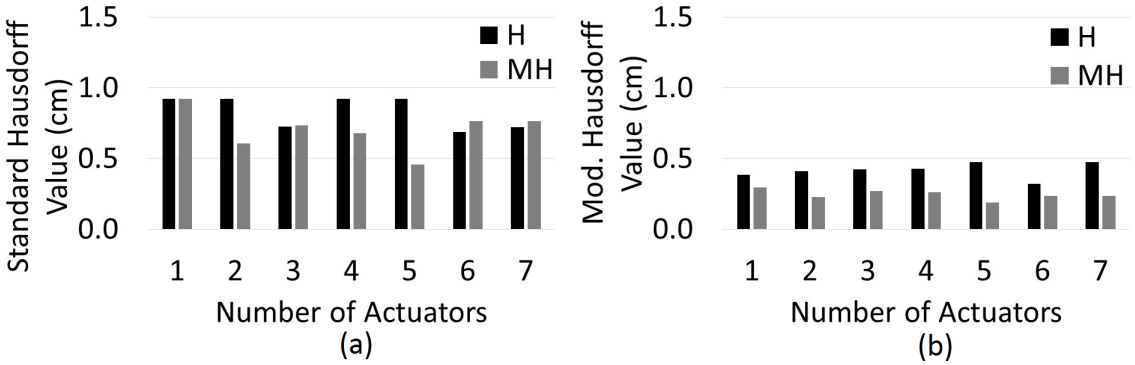

Fig. 10. (a) Standard Hausdorff distance value and (b) Modified Hausdorff distance for optimal designs using various numbers of actuators for design solutions minimizing with respect to the Standard Hausdorff and Modified Hausdorff distances for Target Shape 3.

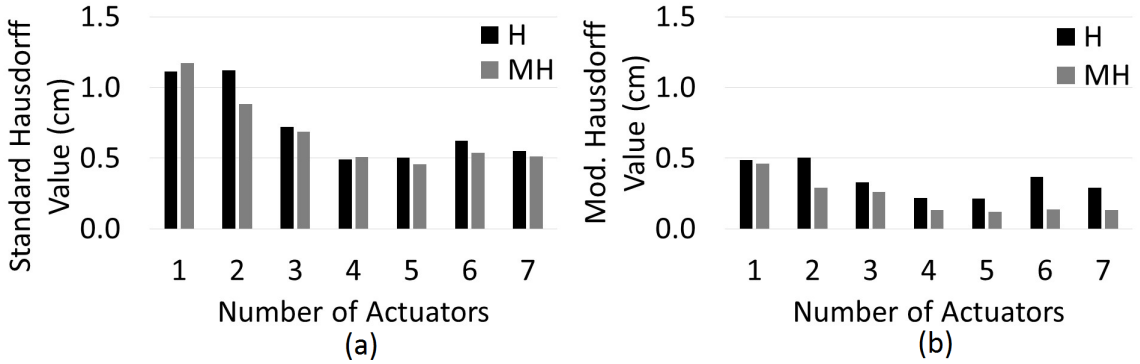

Fig. 11. (a) Standard Hausdorff distance value and (b) Modified Hausdorff distance for optimal designs using various numbers of actuators for design solutions minimizing with respect to the Standard Hausdorff and Modified Hausdorff distances for Target Shape 4.

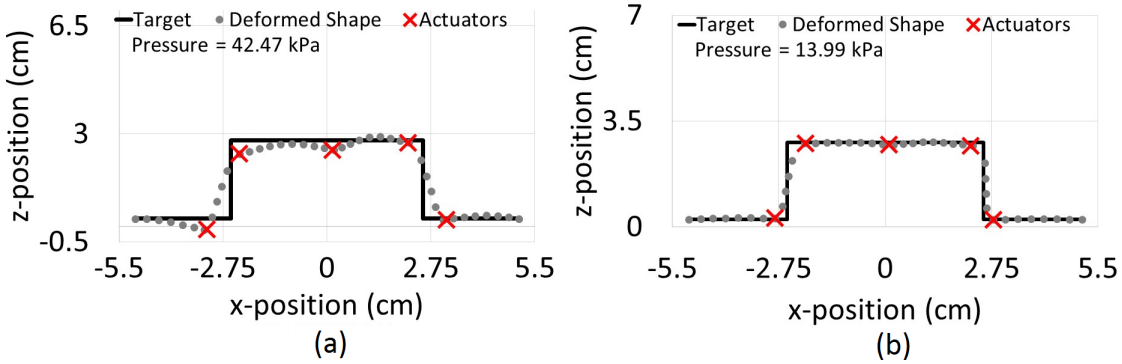

Fig. 12. The morphed tile shape for the “best" design solution, target shape, and actuator placement for the optimization using (a) the Standard Hausdorff distance and (b) the Modified Hausdorff distance for target shape 3.

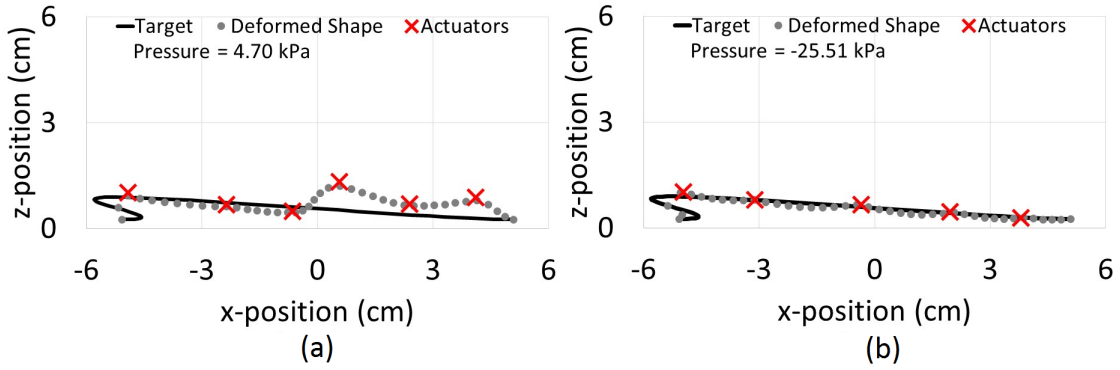

Fig. 13. The morphed tile shape for the “best" design solution, target shape, and actuator placement for the optimization using (a) the Standard Hausdorff distance and (b) the Modified Hausdorff distance for Target Shape 4.

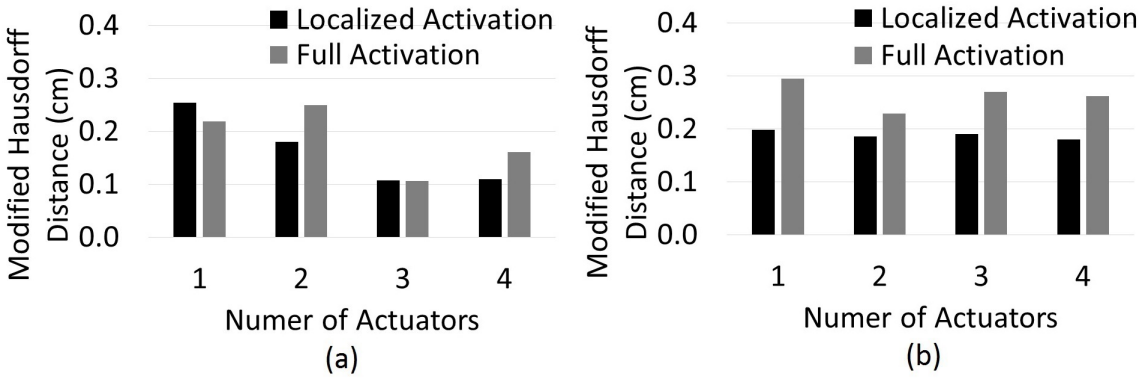

Fig. 14. Modified Hausdorff distance values for optimal designs for Target Shape 2 (a) and Target Shape 4 (b) using various numbers of actuators with both localized activation (black) and full activation (gray).

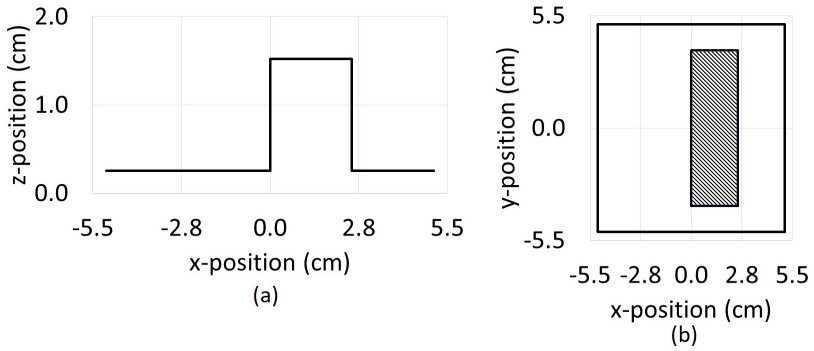

Fig. 15. (a) A cross-sectional view and (b) a top view for the target shape with two directions of spatial variation (a boxcar function), with the hatched section being the raised portion of the target shape.

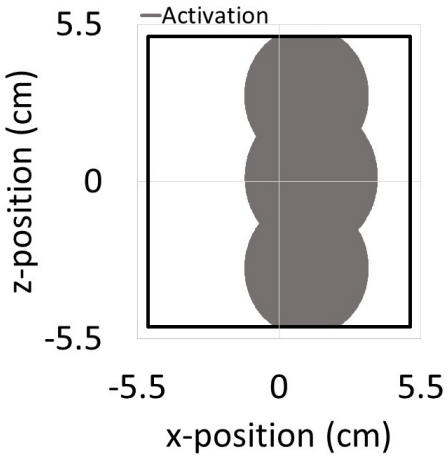

Fig. 16. The activated (gray) and unactivated (white) portions of the tile for the final design solution for the 3D target shape.

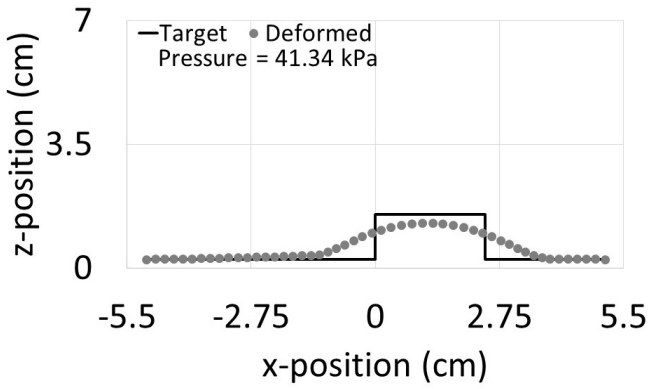

Fig. 17. The morphed tile shape for the design solution and 3D target shape.

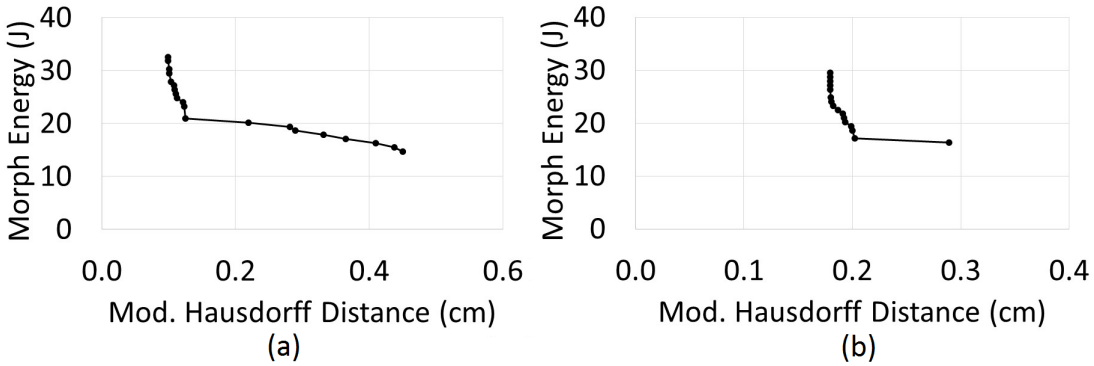

Fig. 18. Trade-off between the two objective functions, the Modified Hausdorff distance (x-axis) and morphing energy cost (y-axis) for Target Shape 2 (a) and Target Shape 4 (b).

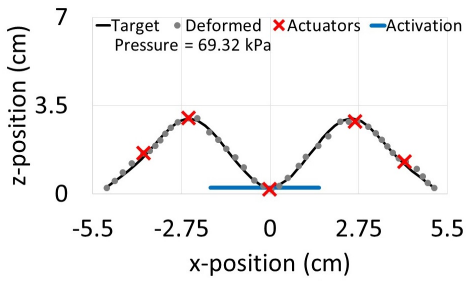

Fig. 19. The morphed tile shape for the “best" design solution, target shape, and actuator placement (a) as well as the thermally activated zones (b) for Target Shape 2.

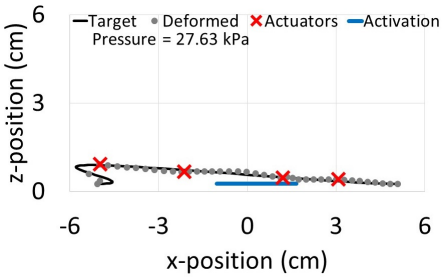

Fig. 20. The morphed tile shape for the “best" design solution, target shape, and actuator placement (a) as well as the thermally activated zones (b) for Target Shape 4.